Observation of a stable fractionalized polar skyrmionlike texture with giant piezoelectric response enhancement

Fangping Zhuo[1,*] and Chan-Ho Yang[1,2,†]

[1]*Department of Physics, and Center for Lattice Defectronics, Korea Advanced Institute of Science and Technology (KAIST), Daejeon 34141, Republic of Korea*

[2]*KAIST Institute for the NanoCentury, KAIST, Daejeon 34141, Republic of Korea*

(Received 8 January 2020; revised 6 October 2020; accepted 1 December 2020; published 18 December 2020)

We report the creation of stable fractionalized polar skyrmionlike structures via flexoelectric effect in a prototypical multiferroic $BiFeO_3$ thin film, which are directly imaged by angle-resolved piezoresponse force microscopy technique. We also demonstrate an approach to enhance piezoresponse at the nanoscale. Phase-field simulations reveal that a tip-driven flexoelectric effect allows the formation of an ordered polar skyrmionlike configuration that is topologically protected by the converse flexoelectric effect. Our findings open up avenues for designing and controlling spatially localized topological textures in rhombohedral ferroelectrics, and also could contribute to future developments for ferroelectric-based nanoelectronic devices.

DOI: 10.1103/PhysRevB.102.214112

I. INTRODUCTION

Topological defects [1–3] can be found in ordered media, for example, ferroic materials with spontaneous magnetization or electric polarization. Ferroelectric topological structures such as vortices [4–6], flux-closure quadrants [7–11], merons [12], and skyrmions [3,13,14] are attracting much attention for their unique insights they give into nontrivial topological physics and great potential for nanodevices, because of the use of ferroelectric polar textures that are much smaller than their counterparts in magnets as functional elements. The related polar vortices or flux-closure configurations have been discovered and studied in ferroelectrics within geometrical nanostructures [4–18], but the spontaneous formation, stabilization, and fractionalization of emergent polar skyrmions have not been satisfactorily understood. A hindrance to precisely investigating polar skyrmion textures in ferroelectrics is the absence of intrinsic chiral interactions (in most cases, known as the Dzyaloshinskii-Moriya interactions), which play a critical role in obtaining such configurations in magnets [19]. Recent experimental and theoretical studies suggest that polar skyrmions can be stabilized in a $PbTiO_3-SrTiO_3$ superlattice [20] or a ferroelectric nanocomposite [21] through the manipulation of lattice-mismatch strain and/or free energies (elastic, electrostatic, depolarization, and gradient energies). This raises the challenging question of whether a fractionalized polar skyrmion, which leads to the topological "fractionalization," i.e., a spatial separation of conventional (integer) polar skyrmions, can be created and stabilized in a spatially uniform ferroelectric material. Direct observation and study of configurable polar skyrmions and topologically similar textures in ferroelectrics will provide the opportunity for disclosing the universal topological features and a pathway for the further advancement of ferroelectrics toward engineering functionalities.

The flexoelectric effect—a linear coupling between electric polarization and strain gradient—is ubiquitous in all materials and can be enhanced at the nanoscale due to the length scaling of strain gradients [22,23]. This offers a powerful route for switching electric polarization and achieving excellent physical properties such as local conduction, photocurrent, photovoltaic, and piezoelectric response [24–28]. In recent years, the strain-gradient-induced effect has been considered as a source for the generation of topological ferroelectric structures [6,29,30]. By recognizing the crucial role of flexoelectricity, we hypothesize that there is a considerable possibility for the formation of deformed polar skyrmionlike structures in a ferroelectric material by using an atomic force microscope (AFM) tip-induced flexoelectric effect.

As illustrated in Fig. 1(a), a symmetrical polar skyrmion with polarizations rotating in a plane perpendicular to the domain boundary can generate a vortex with a winding number (w) of $+1$, where the polarization vectors rotate in the radial planes from the center to the periphery. If we rotate each polarization of the conventional Néel-type polar skyrmion around the in-plane [$\bar{1}10$] axis by $\theta_0 = +54.7^\circ$ so that the polarizations in the matrix region point toward the [111] direction, a deformed skyrmion structure emerges, as schematically shown in Fig. 1(c). Such a homotopic deformation can simultaneously produce a vortex-antivortex pair and asymmetrical distribution of skyrmion number density [compare Fig. 1(d) with Fig. 1(b)]. The skyrmion number density near a vortex core ($w = +1$) is larger than that near an antivortex ($w = -1$). The topological skyrmion number (N) of vortex and antivortex parts has fractional $\frac{-1-\cos[\theta_0]}{2}$ ($= -0.7887$) and $\frac{-1+\cos[\theta_0]}{2}$ ($= -0.2113$), respectively, so the total charge sum of the deformed texture is equivalent to a skyrmion with

*fangpingzhuo@kaist.ac.kr
†chyang@kaist.ac.kr

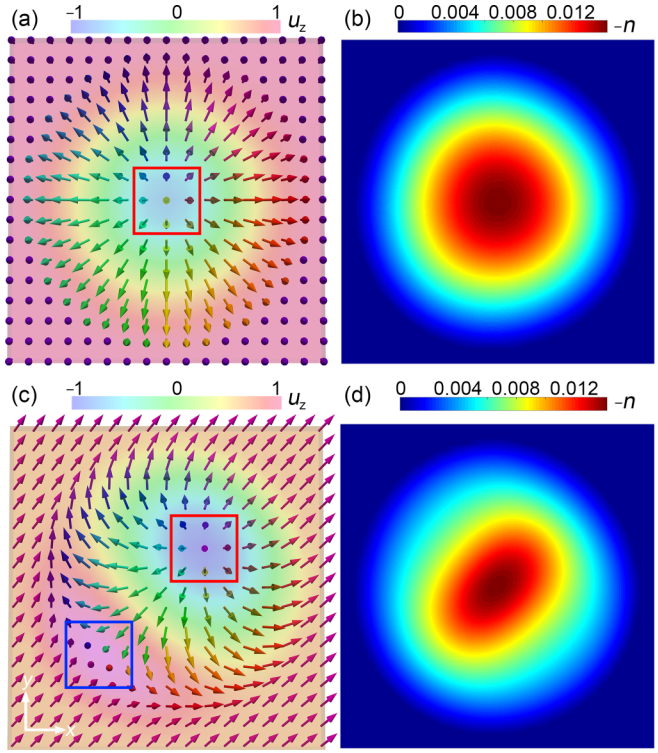

FIG. 1. Schematic illustrations of a polar skyrmion (a) with symmetrical topological density (b), and a fractionalized skyrmion (c) with asymmetrical deformed topological density (d) constructed by rotating all the polarizations of the conventional skyrmion equally so that the polarizations in the matrix region point toward the [111] direction. The topological charge density (n) is given by $n = \frac{1}{4\pi}\boldsymbol{u} \cdot (\frac{\partial \boldsymbol{u}}{\partial x} \times \frac{\partial \boldsymbol{u}}{\partial y})$, where $\boldsymbol{u}$ is the local dipole moment, namely, $\boldsymbol{u} = \mathbf{P}/|\mathbf{P}|$ with $\mathbf{P}$ being the polarization vector. The skrymion number (N) is calculated by an integer index, $N = \int\int n dx dy$. The arrows are colored by polar angle of polarization vector for (a), (c), and the scale bar indicates the out-of-plane unit polarization (u_z). Red and blue loops represent the position of a vortex ($w = +1$) and an antivortex ($w = -1$), respectively. The total topological number of the new texture can be expressed as $N = p_V w_V + p_A w_A$, where $p_V(p_A)$ and $w_V(w_A)$ refer to the polarity and winding number of the vortex (antivortex), respectively. We choose the $+z$ direction to be upward, so both skyrmions in (a), (c) are stable topological textures with $N = -1$.

$N = -1$ (see the Supplemental Material [31] for details). The coexistence of in-plane (IP) and out-of-plane (OOP) polarization components allows fractional topological charges. The presence of ordered vortex-antivortex pair configuration, which exhibits approximatively continuous polarization rotation, is a feature thought to yield large piezoelectricity [32,33]. Since the stress and strain gradients induced by an AFM tip are manifested at the nanoscale, the piezoelectric effect—a linear coupling between electric polarization and strain—is not negligible. This addresses the fundamental questions: (1) What is the relative contribution from flexoelectricity in the creation of a fractionalized polar skyrmionlike structure; (2) to which extent the created fractionalized polar skyrmionlike structure is stable; (3) whether a large piezoresponse can be realized.

In this paper, we explore the creation and stabilization of room-temperature fractionalized polar skyrmionlike topological objects and the interrelationship between the tip-induced flexoelectricity and piezoelectricity in a prototype of multiferroic $BiFeO_3$ (BFO) thin film. We find that the flexoelectric fields induced by an AFM tip-forced inhomogeneous deformation lead to a rotated polarization distribution, which can act as the driver for the formation of stable fractionalized polar skyrmionlike textures. Moreover, a giant enhancement (∼70%) and selective control of local piezoresponse have been realized.

II. RESULTS AND DISCUSSION

Piezoresponse force microscopy (PFM) is now one of the mainstream tools for imaging and manipulating the polarization switching pathway, and is capable of discerning the OOP and IP components of piezoresponse vectors, which allows us to reconstruct the three-dimensional (3D) piezoresponse vectors at the nanoscale [22,34,35]. The lateral resolution of the PFM for domain imaging can be sufficient to observe textures in the ∼100-nm size as was demonstrated for BFO thin films [6,16,24,34–37]. The experiments were performed at room temperature on a ∼50-nm-thick rhombohedral phase BFO epitaxial film grown on a $SrRuO_3$- buffered (110) orthorhombic $DyScO_3$ substrate; see methods and x-ray diffraction data in Fig. S1 of the Supplemental Material [31]. The as-grown high-quality BFO sample has an atomically flat surface with uniformly downward polarization variants (Fig. S3 of [31]). The IP PFM piezoresponse images suggest that the as-grown sample has a stripe domain pattern with 71° domain walls, which is visualized and reconstructed by using the high-resolution lateral angle-resolved PFM technique (see methods and Figs. S4 and S5 of [31]). Details of our angle-resolved PFM technique can be found elsewhere [16,24,36]. We employed a negative voltage (−8 V) to get a monodomain region with polarization pointing toward the [111] direction (Fig. S6 of [31]) as a good platform for conducting the local mechanical switching of ferroelectric polarization.

After applying 4-μN mechanical load at five points by an AFM tip in the upwardly poled area, inhomogeneous surface deformations are locally created [Fig. 2(a)]. Such inhomogeneous deformations generate a large strain gradient, which is most likely to produce large modulations in the flexoelectric field and induced electric polarization [38]. To experimentally implement our concept for a fractionalized polar skyrmionlike structure, within the conventional Hertzian contact model [39–41] (and see also Refs. [27,42,43]), we calculate the flexoelectric field distributions with a static tip force of 4 μN (see Sec. 4 of the Supplemental Material [31] for details). The maximum value of downward OOP flexoelectric field is reached beneath the center of the tip-surface contact area, whereas the anisotropic IP flexofield attains peaks around the contact edges. Our simulation results show that the IP flexofield is comparable to (or even higher than) the OOP flexoelectric field, which plays a critical role in the rotation of IP polarization component.

Direct observation of the created polar quasiparticles is essential for investigating our idea and interpreting the details of topological features. By performing the high-resolution lateral

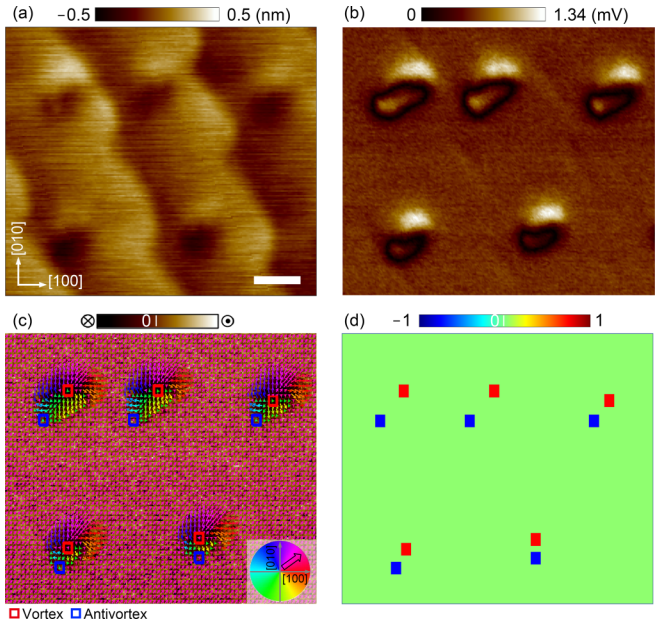

FIG. 2. (a) Topographic image of the BFO sample after 4-μN mechanical load (scale bar: 100 nm). The upper part of the created object is protruding while the other part is lowered in height. (b) Map of IP PFM amplitude signal strength measured at the cantilever orientation toward [100]. (c) Map of the IP piezoresponse vectors. The background contrast refers to the OOP PFM signal. The bright and dark contrasts represent the polarizations toward the upward and the downward, respectively. The arrow color denotes the direction of the IP piezoresponse vectors, as indicated in the color disk legend at the bottom right corner. Each pixel with an arrow in (c) represents an area of $9\times9\,\mathrm{nm}^2$. (d) Map of the winding number. The locations of the singular points are clearly identified by local winding number calculation.

angle-resolved PFM over the same area (see Figs. S7 and S8 of [31] for PFM images and a map of R^2), we are able to obtain the IP PFM piezoresponse signals [Fig. 2(b)] and construct a map of the local IP piezoresponse vectors [Fig. 2(c)]. The created distinct circular polarization configurations have a vortex at the center of them and an antivortex-vortex pair along the [110] direction, where the polarization vectors rotate radially. The two-dimensional (2D) winding number counts the topological singularities in vector fields [6,44]. Therefore, we quantitatively identify the presence of vortex and antivortex in the map of winding number, as displayed in Fig. 2(d). The polarization rotation around the vortex-antivortex pairs in detail can be seen in Fig. S9 of [31]. The winding number is conserved in the in-plane ferroelectrics; thus with a homogeneous background (a monodomain structure with $w = 0$), artificial creation of a polar vortex ($w = +1$) must be spontaneously accompanied by an antivortex ($w = -1$) to conserve the net sum of the winding number of zero. We show that the vortex-antivortex pairs can be experimentally embedded in a uniform monodomain background via tip-induced flexoelectric effect [compare Fig. 2(c) with Fig. 1(c)] under the topological protection, and also be imaged by using the winding number analysis and the unique visualization approach.

To elucidate the structure of the proposed fractionalized polar skyrmionlike topological object, we carried out mapping of 3D piezoresponse vectors. Reconstruction of the 3D polarization textures in a 2D space, see Fig. 3(a) and Fig. S10 of [31] for details, reveals deformed polar skyrmionlike structures containing Bloch-type walls. The asymmetrical skyrmion number density distributions [see Fig. S12(c) of [31]) also confirm the deformed features. All of them have the same IP component handedness, i.e., the same chirality. It is also interesting to note that the created polar textures manifest a total topological charge number of -1, demonstrating that they are topologically equivalent to each other. Moreover, these polar skyrmionlike structures can be stabilized in the system after 24 h (Fig. S11 of [31]). Provided that the polarization correlates with the 3D piezoresponse vector, we may qualitatively recognize the distribution of local total bound charge density (ρ_b^*). According to the divergence theorem [24], the putative bound charge (Fig. S12 of [31]) of each topological polar skyrmion is calculated to be $\sim$0 by integrating the ρ_b^* in the space. Compared with flux-closure domain patterns with four clear domain walls, in-plane PFM contrasts have rather uniform sizes and circular shapes. The size of $\sim$100 nm seems to be related to the film thickness ($\sim$50 nm in our case), which is significantly larger than the meron structure observed in a 5-nm-thick $PbTiO_3$ film [12]. Our results offer an additional example for polar nanodomains such as flux closures [9–11] and bubbles [45]. It could be interesting to further clarify the atomic structure of created textures using other imaging techniques with higher resolution—for example, atomic-scale transmission electron microscopy [12,20]. In this work, strain gradient through the AFM tip load thus provides an alternative route for the active manipulation of ferroelectric domains with local rotated polarization, and also offers an opportunity for discovery and exploitation of intriguing physical properties at the nanoscale (particularly piezoelectricity).

The polarization rotation in piezoelectric materials results in rich functionalities, which include large dielectric permittivity, significant piezoelectricity, and ultrahigh-electromechanical coupling coefficient [32,33,46–48]. For this, we determined the local piezoresponse vector as a function of position in a 2D space. By combining the OOP and IP PFM signals, we are able to map out the 3D piezoresponse vectors through the calibration process (see methods in the Supplemental Material [31]). Here the selective modulation of local piezoresponse has been achieved, as displayed in Fig. 3(b). Note that the antivortex region (state 1) has low piezoresponse (even no piezoelectric activity), whereas the upper region of the vortex core (state 3) shows a remarkable enhancement in piezoresponse (two times as large as that of the rhombohedral phase BFO matrix denoted as state 2). The corresponding line profile of the piezoresponse as a function of position gives detailed information, as plotted in Fig. 3(c). The maximum magnitude of piezoresponse (70 pm/V) is far larger than that of mixed-phase BFO ($\sim$40 pm/V) in the literature [24]. The piezoelectric coefficient, d_{33}, is defined as the volume change of a piezoelectric material under an external electric field [47]. The measured local d_{33} hysteresis loops are used to examine the piezoresponse of these states, as given in Fig. 3(d). An enhancement in d_{33} of $\sim$70% is demonstrated at state 3 when comparing with the BFO matrix (state 2), while a suppression in d_{33} is observed at state 1. Our work

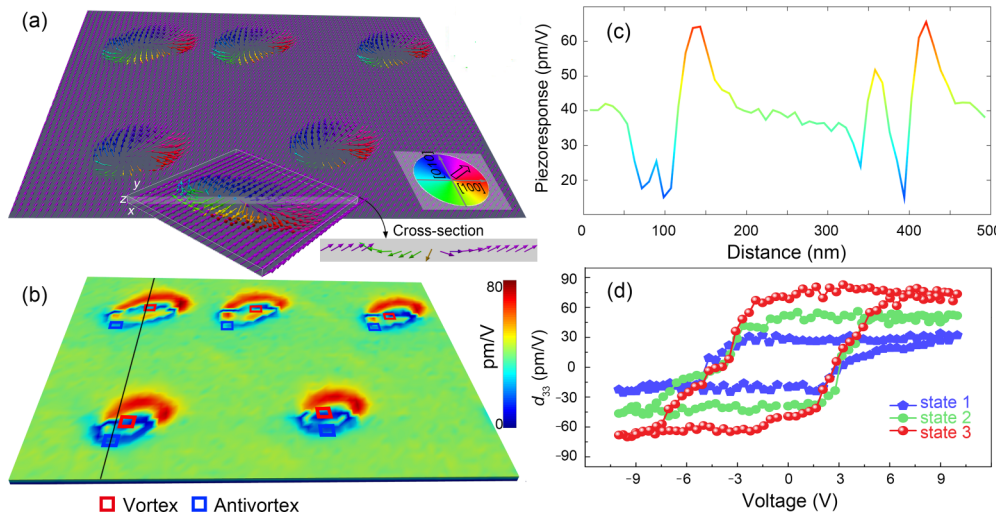

FIG. 3. (a) 3D reconstruction of the polar skyrmionlike textures. Local 3D piezoresponse vectors can be obtained from the OOP and IP PFM signals through the calibration process. The 3D piezoresponse vectors are mapped out in 2D space. The inset shows a normalized skyrmion like texture and a cross section of the polarization based on the upper-left one observed experimentally. (b) Map of the amplitude of 3D piezoresponse vectors. The vortex and antivortex are mapped over the surface image of local piezoresponses. (c) Line profile of piezoresponses along the vertical black line as given in 3(b). (d) The d_{33} loop measured at the different states (state 1: at the antivortex position; state 2: rhombohedral-phase BFO matrix; state 3: around the enhanced piezoresponse region). An enhanced d_{33} value is observed, whereas a lower d_{33} value is measured at the location of the antivortex core.

formulates a rule in the deterministic selection of nanoscale piezoresponse in ferroelectrics, and can also be generalized to the wider class of piezoelectric materials toward high piezoelectricity.

To further explain microscopic details of these stable polar-skyrmionlike structures and the mechanism of selective modulation of local piezoresponse in BFO, we carried out phase-field simulations [49–56]. All the parameters are collected from the literature [22,24,50,54,57] and also listed in Table S1 of [31]. With these calculations, we show that stabilization of the polar skyrmionlike structures can be achieved and they have the condensation of a deformed polarization pattern in the $x-y$ plane and a characteristic total topological charge number of -1 and fractional skyrmion numbers near the vortex and antivortex; see Supplemental Material, Figs. S14(a) and S14(b) [31]. The fractionalized polar skyrmionlike texture in this work has a strong strain gradient as well as a polarization gradient. Nonetheless, the appearance of the skyrmionlike texture means a phenomenological converse flexoelectric energy term that couples polarization gradient to strain plays an important role in decreasing the total free energy or creating a metastable state; see Figs. S14 and S15 and discussions in the Supplemental Material [31]. The flexoelectric effect acts as the driving force for the formation of a noncollinear interaction. Locally unstable structures may appear due to the global advantage of stabilizing an entire topological texture. The fractionalized polar skyrmionlike structures are relatively stable and protected due to their topologically nontrivial nature, similarly to the other topological skyrmionic states that have been discovered and predicted in chiral magnets [2,19], elementary particle physics [58], and Bose-Einstein condensates [59] or liquid crystals [60].

The IP component of the tip-induced polarization has only a component parallel to the [110] direction (that is, IP polarization direction of a rhombohedral phase BFO matrix) at the upper right part, of which the polarization direction can continuously rotate around the vortex. Such a continuous polarization rotation leads to an important consequence: A low-energy barrier exists for polarization switching. This contributes to a piezoelectric response enhancement subjected to the applied electric field and stress. The strong position dependence of the piezoelectric response [see Fig. 3(a)] necessitates directional control of the tetragonal-like phase with spontaneous polarization along the {100} directions. The tip-induced localized tetragonal-like phase can be observed in the piezoresponse vector maps [Figs. 2(c) and 3(a)]. It has been experimentally demonstrated that AFM tip force is sufficient to induce nanoscale morphortropic phase boundary with the coexistence of tetragonal and rhombohedral phases in a BFO thin film; see, e.g., Refs. [27,30]. Our simulation and experimental data do not exclude the premier rhombohedral/tetragonal-like phase coexistence regions in general piezoelectric materials as the origin of the enhanced piezoresponse [33]. However, at the bottom left corner, the tip-induced polarization displays a component antiparallel to the [110] direction. Around the antivortex core, the formation of the charged domain wall contributes to a significant increase in the electrostatic energy near this charged domain wall [61]. Therefore, this electrostatic repulsion, from the growing charged domain wall, increases the local modulus of the BFO film. Our simulation results [see Fig. S14(f) for the ε_{zz} along the normal for a topological texture] also show a small strain around the antivortex. In this case, the polarization switching is hard to produce strain response under an electric field, leading to a low piezoelectric response. It is noteworthy that strictly speaking large piezoelectric activity not only requires a polarization rotation but also the reduction of domain size [62] and the lattice softening [63].

III. CONCLUSIONS

In summary, we created intriguing fractionalized skyrmionlike polarization configurations in a rhombohedral ferroelectric BFO film using a tip-induced flexoelectric effect. By directly observing the piezoresponse vector map and performing phase-field simulations, we identified and examined the created fractionalized polar skyrmionlike textures through local winding number and topological charge number calculations. We showed that the mechanical approach via a flexoelectric field is an effective way to achieve stable polar textures with fractional skyrmion numbers. A giant enhancement and position dependence of local piezoelectric responses were observed, which may be a strategy for enhancing the piezoelectricity. Our findings not only offer a useful concept for tailoring the ferroelectric orders and topological features in complex materials, but also address a solution for technologically important piezoelectric nanodevices. Furthermore, if the dynamic motion of polar skyrmionlike textures can be realized and manipulated by applying an external electric field or magnetic field (for instance, theoretical predictions in Refs. [21,64]), they could be employed to develop skyrmion-based novel functional devices.

ACKNOWLEDGMENTS

This work was financially supported by National Research Foundation (NRF) grants funded by the Korean Government via the Creative Research Initiative Center for Lattice Defectronics (2017R1A3B1023686) and the Center for Quantum Coherence in Condensed Matter (2016R1A5A1008184).

[1] N. D. Mermin, Rev. Mod. Phys. **51**, 591 (1979).
[2] J. Seidel, *Topological Structures in Ferroic Materials* (Springer, Cham, Switzerland, 2016).
[3] F.-T. Huang and S.-W. Cheong, Nat. Rev. Mater. **2**, 17004 (2017).
[4] N. Balke, B. Winchester, Wei Ren, Y. H. Chu, A. N. Morozovska, E. A. Eliseev, M. Huijben, R. K. Vasudevan, P. Maksymovych, J. Britson, S. Jesse, I. Kornev, R. Ramesh, L. Bellaiche, L. Q. Chen, and S. V. Kalinin, Nat. Phys. **8**, 81 (2012).
[5] A. K. Yadav, C. T. Nelson, S. L. Hsu, Z. Hong, J. D. Clarkson, C. M. Schlepütz, A. R. Damodaran, P. Shafer, E. Arenholz, L. R. Dedon, D. Chen, A. Vishwanath, A. M. Minor, L. Q. Chen, J. F. Scott, L. W. Martin, and R. Ramesh, Nature (London) **530**, 198 (2016); **534**, 138(E) (2016).
[6] K.-E. Kim, S. Jeong, K. Chu, J. H. Lee, G.-Y. Kim, F. Xue, T. Y. Koo, L.-Q. Chen, S.-Y. Choi, R. Ramesh, and C.-H. Yang, Nat. Commun. **9**, 403 (2018).
[7] Y. L. Tang, Y. L. Zhu, X. L. Ma, A. Y. Borisevich, A. N. Morozovska, E. A. Eliseev, W. Y. Wang, Y. J. Wang, Y. B. Xu, Z. D. Zhang, and S. J. Pennycook, Science **348**, 547 (2015).
[8] Y. Ivry, D. P. Chu, J. F. Scott, and C. Durkan, Phys. Rev. Lett. **104**, 207602 (2010).
[9] R. K. Vasudevan, Y.-C. Chen, H.-H. Tai, N. Balke, P. Wu, S. Bhattacharya, L. Q. Chen, Y.-H. Chu, I.-N. Lin, S. V. Kalinin, and V. Nagarajan, ACS Nano **5**, 879 (2011).
[10] R. G. P. McQuaid, L. J. McGilly, P. Sharma, A. Gruverman, and J. M. Gregg, Nat. Commun. **2**, 404 (2011).
[11] L.-W. Chang, V. Nagarajan, J. F. Scott, and J. M. Gregg, Nano Lett. **13**, 2553 (2013).
[12] Y. J. Wang, Y. P. Feng, Y. L. Zhu, Y. L. Tang, L. X. Yang, M. J. Zou, W. R. Geng, M. J. Han, X. W. Guo, B. Wu, and X. L. Ma, Nat. Mater. **19**, 881 (2020).
[13] J. M. Gregg, Ferroelectrics **433**, 74 (2012).
[14] M. Dawber, A. Gruverman, and J. F. Scott, J. Phys.: Condens. Matter **18**, L71 (2006).
[15] S. C. Chae, Y. Horibe, D. Y. Jeong, N. Lee, K. Iida, M. Tanimura, and S.-W. Cheong, Phys. Rev. Lett. **110**, 167601 (2013).
[16] J. Kim, M. You, K.-E. Kim, K. Chu, and C.-H. Yang, npj Quantum Mater. **4**, 29 (2019).
[17] L. Li, X. Cheng, J. R. Jokisaari, P. Gao, J. Britson, C. Adamo, C. Heikes, D. G. Schlom, L.-Q. Chen, and X. Pan, Phys. Rev. Lett. **120**, 137602 (2018).
[18] S. Estandía, F. Sánchez, M. F. Chisholm, and J. Gázquez, Nanoscale **11**, 21275 (2019).
[19] U. K. Rößler, A. N. Bogdanov, and C. Pfeiderer, Nature (London) **442**, 797 (2006).
[20] S. Das, Y. L. Tang, Z. Hong, M. A. P. Gonçalves, M. R. McCarter, C. Klewe, K. X. Nguyen, F. Gómez-Ortiz, P. Shafer, E. Arenholz, V. A. Stoica, S.-L. Hsu, B. Wang, C. Ophus, J. F. Liu, C. T. Nelson, S. Saremi, B. Prasad, A. B. Mei, D. G. Schlom *et al.*, Nature (London) **568**, 368 (2019).
[21] Y. Nahas, S. Prokhorenko, L. Louis, Z. Gui, I. Kornev, and L. Bellaiche, Nat. Commun. **6**, 8542 (2015).
[22] P. Zubko, G. Catalan, and A. K. Tagantsev, Annu. Rev. Mater. Res. **43**, 387 (2013).
[23] G. Catalan, A. Lubk, A. H. G. Vlooswijk, E. Snoeck, C. Magen, A. Janssens, G. Rispens, G. Rijnders, D. H. A. Blank, and B. Noheda, Nat. Mater. **10**, 963 (2011).
[24] K. Chu, B.-K. Jang, J. H. Sung, Y. A. Shin, E.-S. Lee, K. Song, J. H. Lee, C.-S. Woo, S. J. Kim, S.-Y. Choi, T. Y. Koo, Y.-H. Kim, S.-H. Oh, M.-H. Jo, and C.-H. Yang, Nat. Nanotechnol. **10**, 972 (2015).
[25] S. M. Park, B. Wang, S. Das, S. C. Chae, J.-S. Chung, J.-G. Yoon, L.-Q. Chen, S. M. Yang, and T. W. Noh, Nat. Nanotechnol. **13**, 366 (2018).
[26] J. Očenášek, H. Lu, C. W. Bark, C. B. Eom, J. Alcalá, G. Catalan, and A. Gruverman, Phys. Rev. B **92**, 035417 (2015).
[27] Y. Heo, B.-K. Jang, S. J. Kim, C.-H. Yang, and J. Seidel, Adv. Mater. **26**, 7568 (2014).
[28] M.-M. Yang, D. J. Kim, and M. Alexe, Science **360**, 904 (2018).
[29] X. Lu, Z. Cheng, Y. Cao, Y. Tang, R. Xu, S. Saremi, Z. Zhang, L. You, Y. Dong, S. Das, H. Zhang, L. Zheng, H. Wu, W. Lv, G. Xie, X. Liu, J. Li, L. Chen, L.-Q. Chen, W. Cao, and L. W. Martin, Nat. Commun. **10**, 3951 (2019).
[30] R. K. Vasudevan, Y. Liu, J. Li, W.-I. Liang, A. Kumar, S. Jesse, Y.-C. Chen, Y.-H. Chu, V. Nagarajan, and S. V. Kalinin, Nano Lett. **11**, 3346 (2011).
[31] See Supplemental Material at http://link.aps.org/supplemental/10.1103/PhysRevB.102.214112 for additional information on

methods, PFM data, Hertzian contact model, details of the phase-field model, and supporting figures and references.
[32] H. Fu and R. E. Cohen, Nature (London) **403**, 281 (2000).
[33] R. Guo, L. E. Cross, S.-E. Park, B. Noheda, D. E. Cox, and G. Shirane, Phys. Rev. Lett. **84**, 5423 (2000).
[34] A. Gruverman, M. Alexe, and D. Meier, Nat. Commun. **10**, 1661 (2019).
[35] R. Lévy and M. Maaloum, Nanotechnology **13**, 33 (2002).
[36] K. Chu and C.-H. Yang, Rev. Sci. Instrum. **89**, 123704 (2018).
[37] Z. Li, Y. Wang, G. Tian, P. Li, L. Zhao, F. Zhang, J. Yao, H. Fan, X. Song, D. Chen, Z. Fan, M. Qin, M. Zeng, Z. Zhang, X. Lu, S. Hu, C. Lei, Q. Zhu, J. Li, X. Gao, and J.-M. Liu, Sci. Adv. **3**, e1700919 (2017).
[38] H. Lu, C.-W. Bark, D. Esque de los Ojos, J. Alcala, C. B. Eom, G. Catalan, and A. Gruverman, Science **336**, 59 (2012).
[39] H. Hertz, J. Reine Angew. Math. **1882**, 156 (1882).
[40] A. C. Fischer-Cripps, *Introduction to Contact Mechanics* (Springer, Boston, 2000).
[41] C. A. Mizzi, A. Y. W. Lin, and L. D. Marks, Phys. Rev. Lett. **123**, 116103 (2019).
[42] O. Marti, B. Drake, and P. K. Hansma, Appl. Phys. Lett. **51**, 484 (1987).
[43] Y. Heo, P. Sharma, Y. Y. Liu, J. Y. Li, and J. Seidel, J. Mater. Chem. C **7**, 12441 (2019).
[44] N. Gao, S.-G. Je, M.-Y. Im, J. W. Choi, M. Yang, Q. Li, T. Y. Wang, S. Lee, H.-S. Han, K.-S. Lee, W. Chao, C. Hwang, J. Li, and Z. Q. Qiu, Nat. Commun. **10**, 5603 (2019).
[45] Q. Zhang, L. Xie, G. Liu, S. Prokhorenko, Y. Nahas, X. Pan, L. Bellaiche, A. Gruverman, and N. Valanoor, Adv. Mater. **29**, 1702375 (2017).
[46] D. Damjanovic, Appl. Phys. Lett. **97**, 062906 (2010).
[47] H. Liu, J. Chen, L. Fan, Y. Ren, Z. Pan, K. V. Lalitha, J. Rödel, and X. Xing, Phys. Rev. Lett. **119**, 017601 (2017).
[48] K. Shimizu, H. Hojo, Y. Ikuhara, and M. Azuma, Adv. Mater. **28**, 8639 (2016).
[49] Z. Hong and L.-Q. Chen, Acta Mater. **152**, 155 (2018).
[50] B. Winchester, P. Wu, and L. Q. Chen, Appl. Phys. Lett. **99**, 052903 (2011).
[51] P. V. Yudin and A. K. Tagantsev, Nanotechnology **24**, 432001 (2013).
[52] Y. Gu, Z. Hong, J. Britson, and L.-Q. Chen, Appl. Phys. Lett. **106**, 022904 (2015).
[53] C. Kittel, *Introduction to Solid State Physics* (Wiley, New York, 1986).
[54] F. Xue, Y. Gu, L. Liang, Y. Wang, and L.-Q. Chen, Phys. Rev. B **90**, 220101(R) (2014).
[55] J. X. Zhang, D. G. Schlom, L. Q. Chen, and C. B. Eom, Appl. Phys. Lett. **95**, 122904 (2009).
[56] L. L. Ma, W. J. Chen, B. Wang, W. M. Xiong, and Y. Zheng, J. Phys.: Condens. Matter **32**, 035402 (2020).
[57] Y.-H. Chu, Q. Zhan, L. W. Martin, M. P. Cruz, P.-L. Yang, G. W. Pabst, F. Zavaliche, S.-Y. Yang, J.-X. Zhang, L.-Q. Chen, D. G. Schlom, I.-N. Lin, T.-B. Wu, and R. Ramesh, Adv. Mater. **18**, 2307 (2006).
[58] T. H. R. Skyrme, Nucl. Phys. **31**, 556 (1962).
[59] U. Al Khawaja and H. T. C. Stoof, Nature (London) **411**, 918 (2001).
[60] D. Foster, C. Kind, P. J. Ackerman, J. B. Tai, M. R. Dennis, and I. I. Smalyukh, Nat. Phys. **15**, 655 (2019).
[61] J. C. Agar, B. Naul, S. Pandya, S. van der Walt, J. Maher, Y. Ren, L.-Q. Chen, S. V. Kalinin, R. K. Vasudevan, Y. Cao, J. S. Bloom, and L. W. Martin, Nat. Commun. **10**, 4809 (2019).
[62] T. Sluka, A. K. Tagantsev, D. Damjanovic, M. Gureev, and N. Setter, Nat. Commun. **3**, 748 (2012).
[63] M. Iwata, H. Orihara, and Y. Ishibashi, Ferroelectrics **266**, 57 (2002).
[64] D. M. Juraschek, Q. N. Meier, M. Trassin, S. E. Trolier-McKinstry, C. L. Degen, and N. A. Spaldin, Phys. Rev. Lett. **123**, 127601 (2019).